Translational Oncology
www.transonc.com

Volume 6 Number 2 April 2013 pp. 133–142 133

DW-MRI as a Predictive Biomarker of Radiosensitization of GBM through Targeted Inhibition of Checkpoint Kinases[1]

Terence M. Williams*, Stefanie Galbán[†,‡], Fei Li[†,§], Kevin A. Heist[†,§], Craig J. Galbán[†,§], Theodore S. Lawrence[‡], Eric C. Holland[¶], Tami L. Thomae[†,§], Thomas L. Chenevert[†,§], Alnawaz Rehemtulla[†,‡,§] and Brian D. Ross[†,§]

*Department of Radiation Oncology, The Ohio State University, Columbus, OH; [†]The Center for Molecular Imaging, University of Michigan Medical Center, Ann Arbor, MI; [‡]Department of Radiation Oncology, University of Michigan Medical Center, Ann Arbor, MI; [§]Department of Radiology, University of Michigan Medical Center, Ann Arbor, MI; [¶]Departments of Cancer Biology and Genetics and Neurosurgery and Brain Tumor Center, Memorial Sloan-Kettering Cancer Center, New York, NY

Abstract

PURPOSE: The inherent treatment resistance of glioblastoma (GBM) can involve multiple mechanisms including checkpoint kinase (Chk1/2)–mediated increased DNA repair capability, which can attenuate the effects of genotoxic chemotherapies and radiation. The goal of this study was to evaluate diffusion-weighted magnetic resonance imaging (DW-MRI) as a biomarker for Chk1/2 inhibitors in combination with radiation for enhancement of treatment efficacy in GBM. *EXPERIMENTAL DESIGN:* We evaluated a specific small molecule inhibitor of Chk1/2, AZD7762, in combination with radiation using *in vitro* human cell lines and *in vivo* using a genetically engineered GBM mouse model. DW-MRI and T1-contrast MRI were used to follow treatment effects on intracranial tumor cellularity and growth rates, respectively. *RESULTS:* AZD7762 inhibited clonal proliferation in a panel of GBM cell lines and increased radiosensitivity in p53-mutated GBM cell lines to a greater extent compared to p53 wild-type cells. *In vivo* efficacy of AZD7762 demonstrated a dose-dependent inhibitory effect on GBM tumor growth rate and a reduction in tumor cellularity based on DW-MRI scans along with enhancement of radiation efficacy. *CONCLUSION:* DW-MRI was found to be a useful imaging biomarker for the detection of radiosensitization through inhibition of checkpoint kinases. Chk1/2 inhibition resulted in antiproliferative activity, prevention of DNA damage–induced repair, and radiosensitization in preclinical GBM tumor models, both *in vitro* and *in vivo*. The effects were found to be maximal in p53-mutated GBM cells. These results provide the rationale for integration of DW-MRI in clinical translation of Chk1/2 inhibition with radiation for the treatment of GBM.

Translational Oncology (2013) 6, 133–142

Introduction

Glioblastoma (GBM) is an almost universally fatal disease. Standard treatment of GBM typically involves surgery followed by a combination of radiation and temozolomide-based chemotherapy, which provides the best chance for long-term survival [1]. Radiation is a major component of the standard treatment and has been shown to independently improve survival [2]. DNA damage induced by radiation activates the phosphoinositide (PI) 3-kinase–related family members, ATM and ATR [3], resulting in the activation of serine/threonine

Address all correspondence to: Brian D. Ross, PhD, Department of Radiology, University of Michigan, Biomedical Sciences Research Building, Ann Arbor, MI 48109.
E-mail: bdross@umich.edu

[1]This work was supported by the following grants: National Institutes of Health P01CA085878 (A.R., B.D.R., and T.L.C.), P50CA093990 (A.R. and B.D.R.), and an Radiological Society of North America Research Resident/Fellow grant (T.M.W). T.M.W. has been designated a B. Leonard Holman Pathway Fellow by the American Board of Radiology. B.D.R. and A.R. have ownership interest (including patents) in ImBio, LLC related to the underlying DW-MRI technology.
Received 13 February 2013; Revised 13 February 2013; Accepted 28 February 2013

DOI 10.1593/tlo.13214

effector checkpoint kinases, Chk1 and Chk2. Checkpoint kinase activation causes S and G_2/M arrest [4–7], allowing tumor cells time to undertake DNA repair before reentering mitosis thereby reducing the potential for propagating potentially severe genotoxic damage that would ultimately prove therapeutically beneficial by inducing cell death through various processes including apoptosis, mitotic catastrophe, or postmitotic death. In addition to regulating the cell cycle, Chk1/2 kinases can also affect processes of DNA repair, chromatin regulation, and induction of cell death [8].

An intact G_2/M arrest mechanism can also be mediated by checkpoint kinases in cells, which are p53 nonfunctional. This mechanism has also therapeutic implications as p53 mutations are known to occur at a rate of approximately 25% to 40% and 65% to 80% in primary and secondary GBM, respectively [9,10]. If GBM tumors are deficient in G_1 DNA damage checkpoint pathway as a result of p53 mutations or other events, more reliance will be placed on the S and G_2/M checkpoints for DNA damage repair and survival. Therefore, inhibition of these additional checkpoints is important for effective sensitization of tumor cells to genotoxic therapies.

Stem cell research has provided evidence that CD133 (Prominin-1)–positive GBM cells have heightened capabilities of resolving DNA damage mediated by radiation. In a report by Bao et al., radiation induced an increase in the fraction of surviving cells expressing CD133 both *in vitro* and *in vivo* [11]. In this study, CD133+ cells were found to be more resistant to radiation than CD133− cells through preferential activation of the DNA damage checkpoint pathways and an increase in DNA repair capabilities. Furthermore, a nonspecific inhibitor of Chk1 and Chk2 kinases was found to sensitize CD133+ cells to radiation. These results reveal that Chk1/2 pathways are highly relevant for GBM survival.

The use of quantitative imaging for evaluation of treatment response in mouse orthotopic tumor models is useful for providing sensitive and noninvasive metrics of treatment response. Anatomic images obtained using magnetic resonance imaging scanners have been shown to be useful for delineation of intracerebral glioma volumes in rodents over time and to quantify the response to therapeutic intervention [12]. Moreover, diffusion-weighted magnetic resonance imaging (DW-MRI) has been reported as an imaging biomarker for detection of the cellular changes occurring early within a tumor following an effective cytotoxic treatment [13]. Application of DW-MRI in this context has shown that treatment-induced loss of tumor cellular density will result in an increase in the mobility of tumor water molecules as loss in cell numbers and associated changes in tumor tissue architecture produce a less water diffusion–restricted environment [14]. Application of DW-MRI was initially reported as a biomarker of therapeutic response in 9L glioma-bearing rats treated with a chemotherapeutic agent [12,15] and has rapidly been applied in many clinical studies and over a variety of tumor types [16–19].

In this present study, we hypothesized that inhibition of Chk1 and Chk2 kinases with a selective Chk1/2 inhibitor (AZD7762) would result in GBM radiosensitization. AZD7762 is a potent ATP-competitive inhibitor with IC_{50}s of 5 and <10 nM for Chk1 and Chk2, respectively. AZD7762 has been shown to effectively abrogate DNA damage–induced S and G_2/M checkpoints [20]. We also hypothesized that these effects would predominate in p53-mutated cells. In this report, we show that AZD7762 has *in vitro* and *in vivo* efficacy alone and potentiates the effects of radiation in GBM. These findings provide a strong rationale for evaluating the use of checkpoint kinase inhibitors in combination with current GBM treatment, optimally directed at p53-mutated tumors.

Materials and Methods

Antibodies, Chemicals, and Cell Culture

Anti-cdc25a antibody was purchased from Santa Cruz Biotechnology (Santa Cruz, CA). Anti-Chk1, Chk2, phospho-Chk1 (S345), phospho-Chk1 (S296), phospho-H2AX (S139), phospho-p53 (S15), and GAPDH antibodies were purchased from Cell Signaling Technology (Danvers, MA). Ki67 antibody was purchased from Dako (Carpinteria, CA). AZD7762 was purchased from Axon MedChem (Groningen, The Netherlands). The structure for AZD7762 is shown in Figure 1*A*. For *in vitro* studies, AZD7762 was dissolved in DMSO. For *in vivo* studies, AZD7762 was dissolved in 11.3% 2-hydroxypropyl-β-cylodextrin (Sigma-Aldrich, St Louis, MO) in 0.9% sterile saline, vortexed, stored at 4°C, and used within 14 days. Human U251 cells were grown in Dulbecco's modified Eagle's medium with 10% FBS, D4MG cells in RPMI 1640 with 10% FBS, U87 cells in Dulbecco's modified Eagle's medium with 10% FBS, and SKMG-3 cells in alphaMEM with 10% fetal calf serum and 10 mM Hepes. Cells were grown in a 37°C incubator with 5% CO_2.

Immunoblot Analysis

Cell lysates were prepared immediately in RIPA lysis buffer [1% NP-40, 150 mM NaCl, 50 mM Tris-HCl (pH 7.4), 0.25% Na-deoxycholate, 1 mM EDTA] supplemented with 1× protease inhibitor (cOmplete; Roche Applied Science, Indianapolis, IN) and phosphatase inhibitors (PhosSTOP; Roche Applied Science). Protein concentration was determined with a DC Protein Assay Kit (BioRad, Hercules, CA). Proteins were resolved by sodium dodecyl sulfate–polyacrylamide gel electrophoresis and transferred to nitrocellulose

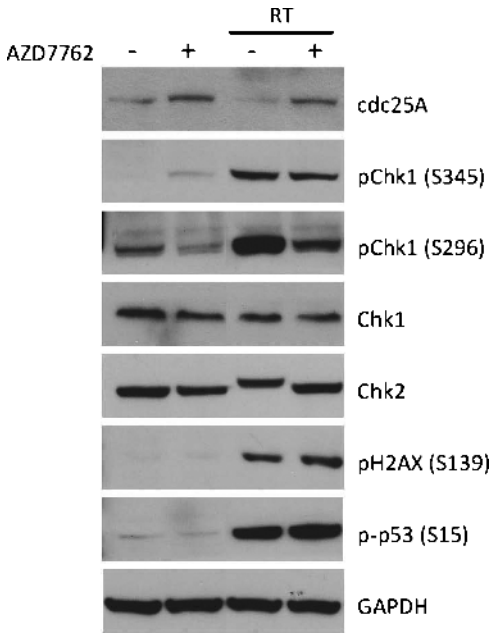

Figure 1. AZD7762 inhibits Chk1 and Chk2 activity in U251 cells. U251 cells were pretreated for 1 hour with DMSO or AZD7762 (100 nM) and treated with and without radiation (6 Gy). Three hours later, cells were lysed and extracts were immunoblotted for cdc25A, phospho-Chk1 (S345 and S296), Chk1, Chk2, phospho-H2AX (S139), and phospho-p53 (S15). GAPDH was shown as equal loading control.

membranes. Primary antibodies were allowed to bind for 2 hours at room temperature and used at a dilution of 1:500 to 1:2000, except for GAPDH that was used at 1:10,000. After washing in TBS-Tween, membranes were incubated with HRP-conjugated secondary antibodies diluted 1:10,000 for 1 hour. Membranes were washed with TBS-Tween and incubated for 1 minute with enhanced chemiluminescence reagent (Amersham Pharmacia, Uppsala, Sweden) before film exposure.

Flow Cytometry

Cells were plated in six-well dishes, pretreated for 1 hour with DMSO or AZD7762, and treated with or without radiation. At 24 hours following radiation exposure, cells were harvested with trypsin, washed with medium, spun down, and resuspended in 1 ml of phosphate-buffered saline (PBS). Cells were immediately fixed for 30 minutes with 9 ml of ice-cold 80% ethanol added slowly with mixing. Cells were washed twice with PBS and resuspended in 1 ml of PBS containing 10 μg/ml propidium iodide and 0.25 mg/ml RNase A. Cells were incubated for 30 minutes and stored in the dark before analysis. Cells were then transferred to 5-ml polystyrene round bottom tubes through cell strainer lids and analyzed on a FACSCalibur (BD Biosciences, San Jose, CA). Data were fit using ModFit LT (Verity Software House, Topsham, ME).

Clonogenic Survival Assays

Cells were trypsinized to generate single-cell suspensions and cells were seeded into six-well or 60-mm tissue culture plates (in triplicate). Cells were incubated with DMSO or AZD7762 for 1 hour before irradiation and kept in DMSO or AZD7762 for a total of 24 hours after radiation before changing the medium. For experiments without radiation, cells were incubated with DMSO or AZD7762 for 24 hours before changing the medium. At 10 to 14 days after seeding, colonies were stained with 0.5% crystal violet, and the numbers of colonies containing at least 50 cells were determined. Plating efficiency, survival fractions, and dose enhancement ratios were calculated according to previously described methods [21]. For each condition, six wells were plated in replicate for experiments performed in six-well plates and in triplicate for experiments performed in 60-mm culture plates. Experiments were repeated multiple, independent times.

In Vivo *Tumor Studies*

We used a well-validated genetically engineered mouse model of GBM [INK4a/ARF(−/−) PTEN(loxP/loxP)/Ntv-a RCAS/PDGF(+)/Cre(+)], which lacks the tumor suppressors INK4A/ARF (p16 and $p19^{ARF}$) and PTEN, with overexpression of PDGF to drive formation of GBM [22,23]. In this model, PTEN is deleted in nestin-expressing cells in an INK4A/ARF-deficient mouse background, and PDGF is overexpressed using RCAS-tva technology. The PDGF-driven model has been shown to exhibit pathologic features similar to the human disease counterpart and represents a proneural model. The lack of $p19^{ARF}$ in this model renders tumor cells functionally *p53 deficient* since ARF normally inhibits the p53 inhibitor Mdm2. More specifically, ARF functions as a tumor suppressor by forming complexes with Mdm2, an E3 ubiquitin ligase that serves as a negative regulator of p53. Upon DNA damage, phosphorylation of Mdm2 allows stabilization and activation of p53 to promote cell cycle arrest and DNA repair. Thus, a vital role of ARF is to activate p53-dependent cell cycle arrest and apoptosis. Because ARF is deleted in this model, Mdm2 activity is high, resulting in p53 dysregulation and relative functional inactivation of p53 in response to DNA damage.

All animal procedures described herein were approved by the University of Michigan Committee for Use and Care of Animals (Protocol No. 09583). The generation of RCAS–PDGF-B and RCAS-Cre–transfected DF1 cells has been previously described [22]. Briefly, 8×10^4 cells were implanted under stereotactic guidance using a 30-gauge needle into the right frontal cortex of transgenic mice at a depth of 3 mm. After implantation, tumor volumes were monitored and calculated using contrast-enhanced T1-weighted MR images. Once tumor volumes reached 20 to 40 μl on pretreatment MRI, animals were randomized to a treatment arm. Animals were monitored carefully and sacrificed at the end of the treatment schedule for histologic analysis.

MRI Evaluation of Tumor Treatment Responses

MRI was performed using a 9.4-T, 16-cm horizontal bore (Agilent Technologies, Inc, Santa Clara, CA) Direct Drive System with a mouse head quadrature volume coil or mouse surface receive coil (m2m Imaging, Corp, Cleveland, OH) actively decoupled to a whole-body volume transmit coil (Rapid MR International, LLC, Columbus, OH). Throughout the MRI experiments, animals were anesthetized with 1% to 2% isoflurane/air mixture, and body temperature was maintained using a heated air system (Air-Therm Heater; World Precision Instruments, Sarasota, FL). MR images were acquired before treatment initiation, then every other day until the animals were sacrificed or became moribund. MR imaging sequences were used in this study to measure tumor volumes over time [12] as well as for quantification of tumor apparent diffusion coefficient (ADC) values [22]. Delineation of tumor from healthy brain tissue was accomplished using contrast-enhanced T1-weighted spin-echo images with the following acquisition parameters: repetition time/echo time = 510/15 ms, field of view = 20 × 20 mm^2, matrix size = 128 × 128, slice thickness = 0.5 mm, 25 slices, and two averages. Total acquisition time was 2 minutes and 12 seconds. An intraperitoneal injection of 50 μl of 0.5 M gadolinium-DTPA (Magnevist; Bayer Healthcare Pharmaceuticals, Wayne, NJ) 5 minutes before image data acquisition was used to provide for contrast enhancement of the tumor.

Tumor ADC maps were derived using a DW spin-echo sequence, equipped with a navigator echo for motion correction and gradient waveforms sensitive to isotropic diffusion, with the following parameters: repetition time/echo time = 4000/37 ms, field of view = 20 × 20 mm^2, matrix size = 128 × 64, slice thickness = 0.5 mm, 25 slices, one average, diffusion time = 40 ms, gradient pulse width = 10 ms, and b values (diffusion weighting) = 120 and 1200 s/mm^2. Total acquisition time was approximately 8.5 minutes. Diffusion scans were used to follow early changes in tumor cellular density during the initial 7 days posttreatment initiation.

For longitudinal quantification of tumor volumes, volumes of interest were contoured along the enhancing tumor rim using the contrast-enhanced T1-weighted images. Tumor volumes were used to follow treatment response for the individual treatments. The tumor regions were also used to derive whole-tumor means of ADC values over time for individual animals. ADC maps were calculated from the two diffusion weightings (b values) using the following equation:

$$\mathrm{ADC} = \frac{\ln\left(\frac{S_1}{S_2}\right)}{(b_2 - b_1)},$$

where S_1 and S_2 are the signal intensities at b values b_1 and b_2, respectively, and ADC is the ADC obtained using b_1 and b_2. Voxels that exhibited insufficient signal, which was defined as <10× noise, in the low b value image (b = 120 s/mm^2) were excluded from the analysis. Image reconstruction and digital image analysis were done using software algorithms developed in Matlab (The MathWorks, Natick, MA).

Early response in mean ADC values was assessed by the area under the curve (AUC) of the mean tumor ADC from baseline to day 5 posttreatment initiation. The AUC from 0 to day 5 was determined by calculating the AUC at incremental time points using the trapezoidal rule and summing over all incremental AUC values, i.e.,

$$\mathrm{AUC} = \sum_i (t - t_{i-1}) \cdot (\mathrm{AUC}_{i-1} + \mathrm{AUC}_i)/2$$

Experimental Radiation

Radiation was performed at 320 kVp and 10 mA using an IC-320 orthovoltage irradiator (Kimtron Medical, Bantam, CT). For *in vitro* experiments, a 20 × 24 cm cone was used at a source-to-surface distance of 50 cm at a dose rate of ~434 cGy/min. For animal irradiation, a 6 × 8 cm cone was used at a source-to-surface distance of 40 cm at a dose rate of ~138 cGy/min. Dosimetry was carried out using an ionization chamber connected to an electrometer system that was directly traceable to a National Institute of Standards and Technology calibration. Mice were anesthetized with a 1% to 2% isoflurane/air mixture and placed in restraining device, and whole brain was irradiated while the rest of the body was shielded using a custom-cut lead secondary collimator. *In vivo* administration of AZD7762 (15 mg/kg) along with radiation therapy (RT; 1 Gy) was given concurrently daily for 5 days a week over a 2-week period.

Immunohistochemistry

At the conclusion of the experiments, intracranial tumors were harvested and fixed in 10% neutral-buffered formalin for at least 48 hours (n = 4 per group). Tumors were sectioned and paraffin embedded, and 5-μm sections were cut onto slides. Paraffin was removed in xylene, and slides were rehydrated through gradually decreasing alcohol concentrations 2 min/step before ending in tap water (100% ethanol, 95% ethanol, 70% ethanol, water). Antigen retrieval was performed by microwaving slides for 10 minutes in pH 6.0 citrate buffer, followed by a 10-minute cooling period and a 10-minute running water wash. Immunoperoxidase staining was performed on a Dako AutoStainer at room temperature by applying peroxidase block (5 minutes), buffer rinse, primary antibody (30 minutes), buffer rinse, secondary antibody (EnVision + anti-rabbit; 30 minutes), buffer rinse, DAB (5 minutes), buffer rinse, followed by hematoxylin counterstain (2 seconds) and water rinse. Slides were then dehydrated through gradually decreasing alcohol concentrations (70% ethanol, 95% ethanol, 100% ethanol, 2 minutes each), three xylene washes (2 minutes each), and followed by placement of a coverslip. Images were captured on an Olympus BX-50 microscope (original magnification, ×4–40).

Data Analysis

Data were presented as mean ± SEM for clonogenic survival and tumor growth experiments. The group comparisons of the percent change in tumor volume were performed at individual time points. Statistical comparisons were made between the control and experimental conditions using the unpaired two-tailed Student's t test with significance assessed at P values < .05.

Results

Effects of AZD7762 on Chk1 and Chk2 Activation and Radiation-Induced G_2/M Arrest

The ability of AZD7762 to inhibit Chk1 and Chk2 activity was initially evaluated *in vitro* using U251 GBM cells. Chk1 is involved in regulation of levels of cdc25A, a phosphatase that controls progression through the cell cycle [8]. Activation of cdc25A allows efficient activation of CDK2, allowing cell cycle progression through various checkpoints. Upon Chk1 activation after DNA damage, Chk1 phosphorylates cdc25A resulting in ubiquitin-mediated cdc25A degradation, allowing cell cycle arrest. As shown in Figure 1, AZD7762 treatment stabilized cdc25A, resulting in an increase in cdc25A levels in U251 cells. In addition, AZD7762 treatment increased phospho-Chk1 (S345), which has been observed previously and appears to be related to amplification of the ATM/ATR-mediated DNA damage response [23]. As expected, radiation alone activated Chk1 and Chk2 as determined by increased levels of phospho-Chk1 (S345 and S296) and decreased gel mobility of Chk2 (indicating increased phospho-Chk2), as well as resulting in increased levels of phospho-p53 (S15) and phospho-gammaH2AX (S139), both markers of DNA damage induced by radiation. Furthermore, the ability to undergo autophosphorylation (S296) was inhibited by AZD77262 both in the presence and absence of radiation, which has been shown previously [23]. Lastly, AZD7762 also abrogated Chk2 activation after radiation, as seen by the loss of the decreased gel mobility of Chk2.

To confirm the effects of AZD7762 on cell cycle progression, we performed flow cytometry on U251 cells. Cell cycle analysis was performed following treatment of U251 cells cultured at the exponential phase of growth with combinations of DMSO, AZD7762, and RT (6 Gy) to determine G_1, S, and G_2/M phase fractions at 24 hours after radiation. For these studies, cells were pretreated for 1 hour with DMSO or AZD7762 before radiation. Twenty-four hours after radiation, cells were fixed, stained with propidium iodide, and analyzed by flow cytometry. As shown in Table 1, radiation induced a G_2/M arrest as expected, resulting from activation of checkpoint kinases and DNA damage repair pathways. Almost no cells were noted in S phase. In the presence of AZD7762, however, there was significant loss of the proportion of cells in G_2/M, indicating that many cells were allowed to prematurely reenter the cell cycle, as noted by increased populations of G_1 and S phase cells.

p53-dependent Effect of AZD7762 on Cell Proliferation and Radiosensitization

A panel of human GBM cell lines consisting of U251, D54MG, U87, and SKMG3 cells was used to evaluate the effects of AZD7762 on proliferation and survival. Clonogenic proliferation assays were

Table 1. Treatment Effects on U251 GBM Cell Cycle.

U251	24 Hours		
	G_1 (%)	S (%)	G_2/M (%)
DMSO	40.0	33.5	26.4
AZD7762	48.0	33.2	18.8
DMSO + RT	12.4	0.0	87.8
AZD7762 + RT	32.8	42.7	24.6

performed by plating equal cell numbers at very low density, incubating with varying concentrations of AZD7762 for 24 hours, and then allowing cells to form colonies (defined as >50 cells) over the next 10 to 14 days. As shown in Figure 2*A*, all cell lines were sensitive to increasing doses of AZD7762, albeit with differential sensitivity. Interestingly, the two p53 mutant cell lines, U251 and SKMG3, had the greatest degree of sensitivity to AZD7762. In fact, SKMG3 cells showed dramatic sensitivity even at concentrations as low as 0.1 μM. However, the two p53 wild-type cell lines showed the most resistance to AZD7762.

Next, radiation clonogenic assays were carried out to test the radiosensitivity of multiple GBM cell lines. Cells were pretreated with AZD7762 for 1 hour followed by increasing doses of radiation, followed by the continued presence of AZD7762 for 24 hours. Of the p53 wild-type cell lines D54MG and U87, no radiosensitization was observed with AZD7762 (data not shown). However, both p53 mutant cell lines U251 and SKMG3 showed significant radiosensitization after treatment with AZD7762, with dose enhancement ratios of 1.25 and 1.44, respectively (Figure 2*B*). These data are consistent with the overall hypothesis that Chk1/2 inhibitors specifically enhance the cytotoxicity of DNA-damaging agents in checkpoint-defective p53 mutant tumors.

Concurrent Treatment with AZD7762 and Radiation Improves Therapeutic Response In Vivo

We initially performed a dose response experiment to test the effect of increasing concentrations of AZD7762 on the tumor growth in this GBM mouse model. We performed MRI screening of mice as previously described [22]. Once intracranial tumors of 20 to 40 μl were identified by screening MRI, mice were randomized to control (vehicle) and 5, 15,

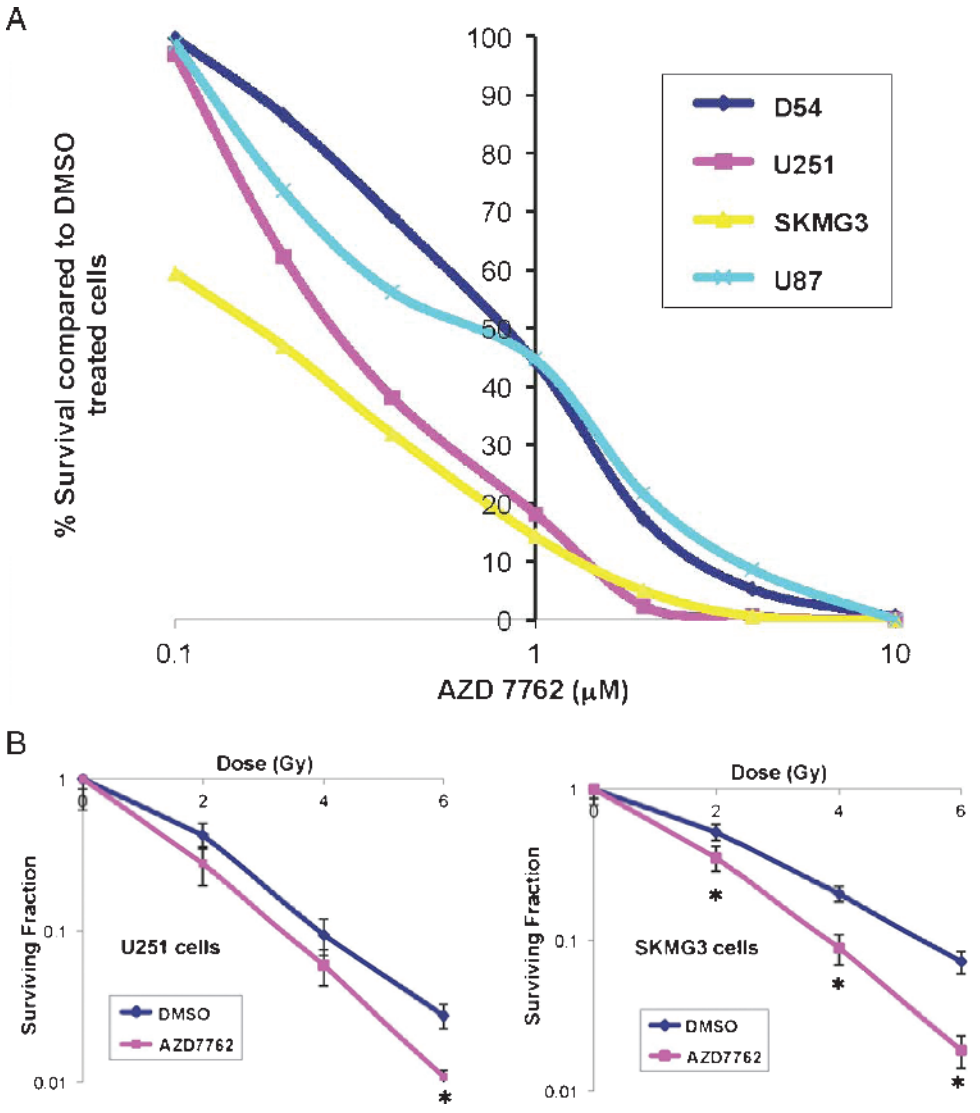

Figure 2. AZD7762 inhibits proliferation and radiosensitizes a panel of GBM cells in a p53-dependent manner. (A) Clonogenic proliferation assays were performed on a panel of GBM cell lines, including U251, D54MG, U87, and SKMG3 cells. Cells were treated with a range of concentrations of AZD7762 for 24 hours and allowed to form colonies after 10 to 14 days. Cells most sensitive to treatment with AZD7762 were the two p53 mutant cell lines, U251 and SKMG3. (B) Clonogenic survival assays were performed by pretreating cells with DMSO or AZD7762 (200 nM) for 1 hour before increasing doses of radiation, then changing the medium 24 hours later and allowing the cell lines to form colonies over 10 to 14 days. AZD7762 treatment resulted in substantial radiosensitization in p53 mutant cell lines U251 and SKMG3 but not p53 wild-type cell lines U87 and D54MG. Asterisks indicate P value $< .05$ compared to DMSO-treated cells. Error bars represent SEM.

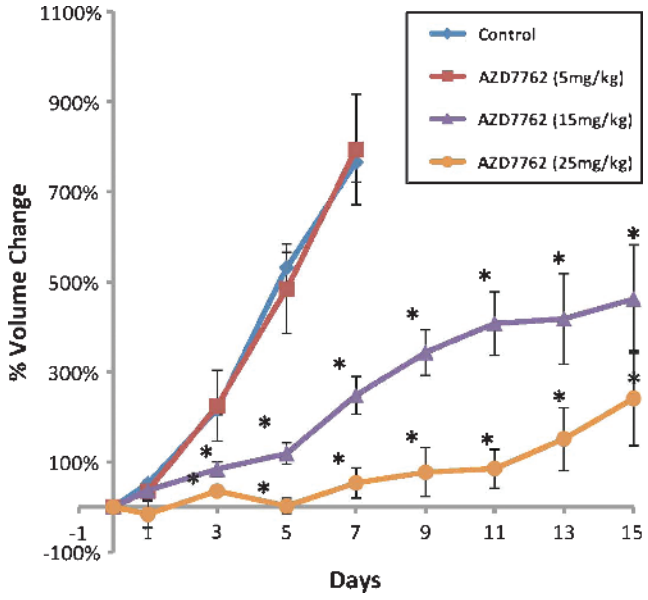

Figure 3. *In vivo* dose response of AZD7762. Mice were randomized to 1) control (vehicle; $n = 7$), 2) 5 mg/kg AZD7762 ($n = 4$), 3) 15 mg/kg AZD7762 ($n = 10$), or 4) 25 mg/kg AZD7762 ($n = 6$). There was a dose-dependent effect with AZD7762 with increasing concentration resulting in higher tumor growth inhibition.

or 25 mg/kg AZD7762 delivered by intraperitoneal injection daily for 2 weeks at 5 days per week. As shown in Figure 3, the 5 mg/kg dose had no significant effect on tumor growth compared with vehicle-treated mice. However, increasing doses of 15 and 25 mg/kg demonstrated a dose-dependent effect of AZD7762 on GBM growth inhibition.

The efficacy of AZD7762 in combination with radiation was evaluated for improvement in tumor control using the PDGF-driven genetically engineered GBM model. Mice were screened until they developed tumors ranging in size from 20 to 40 μl and then randomized to 1) vehicle control, 2) AZD7762, 3) radiation (RT), or 4) AZD7762 concurrent with RT (with AZD7762 administered 1 to 2 hours before radiation). Representative coronal T1 Gd-contrast MR images from each of the treatment arms over 15 days are shown in Figure 4. As shown in Figure 4 and quantified in Figure 4*B*, vehicle-treated tumors grew at a rapid pace increasing about 800% in tumor volume over a 7-day time period during the course of the study. Treatment with radiation or AZD7762 as single therapies significantly inhibited the overall tumor growth rate over control tumors. However, as shown in Figure 4*B*, a larger therapeutic benefit based on larger tumor growth rate inhibition from AZD7767 administration over that of RT alone was observed during the end of the second week of treatment. All tumor volumes were significantly different ($P < .05$) from control tumor volumes beginning at day 3 posttreatment initiation. The combined therapy group was also significantly different ($P < .05$) from the other three groups beginning at day 3 posttreatment initiation. Tumors treated with the combination of AZD7762 and radiation were found to have the most significant therapeutic response. These mice survived the longest, with 22% surviving by the end of the predefined end of the study (23–25 days, mouse with significant neurologic signs, or tumor >150 μl) compared to 0% for all other groups. Importantly, mice were weighed twice weekly and monitored closely during therapy administration and had no significant toxicity with only a maximum 7% decline in body weight in any of the treated groups. Once tumors grew to a large size, all mice began to lose weight likely as a function of decreased neurocognitive ability.

DW-MRI Reveals AZD7762-Mediated Loss of GBM Cellular Density

The AUCs of mean tumor ADC values over the first 5 days of fractionated dose treatment cycle for each treatment group are presented in Figure 5. Control animals were found to have significantly smaller AUC values over this time frame compared to the treatment groups. In contrast, single-agent therapy using RT or AZD7762 both had increased ADC tumor values resulting in a significantly high AUC value over control animals during the first cycle of treatment. Furthermore, while efficacy for both AZD7762 and RT was observed, the combination of AZD7762 and RT was the only treatment group found to have gained control of tumor growth over the 2-week, two-cycle treatment time period (Figure 4*B*). Following one full cycle of treatment with chemoradiation, a significantly higher increase in tumor ADC values was found in the combined treatment group compared to the single-agent treatment groups when the AUCs of the mean ADC values were compared (Figure 5). Thus, the combination therapy group not only had the largest increase in tumor ADC values (Figure 5) but was also found to have the correspondingly most efficacious treatment benefit (Figure 4*B*). It was also noteworthy that following the first treatment cycle from days 0 to 4, tumor ADC values all began to decrease from days 5 to 7 (data not shown). During this time frame, animals were not treated and the drop in diffusion values indicates a probable repopulation of tumor cells occurring during that time interval as increased density of tumor cells would result in a more impeded water diffusion environment within the tumor mass [24]. Tumor ADC maps from representative animals are also shown for each of the five groups at day 5 posttreatment initiation. Tumors treated with single agents exhibited a modest shift in increased diffusion values, whereas the largest effect was found in the combination therapy (RT + AZD7762).

Immunohistochemical Evaluation of In Vivo *GBM Treatment Effects*

To study the effects of AZD7762 on tumor cell proliferation, intracranial tumors were harvested several hours at the conclusion of the overall 2-week study and subjected to immunohistochemistry. Tumors displayed findings similar to human GBM, including nuclear atypia, mitotic figures, areas of necrosis, and vascular/endothelial proliferation as depicted in Figure 6*A*. As shown in Figure 6*B*, control tumors displayed high Ki67 staining indices, consistent with rapid GBM tumor proliferation. Treatment with RT resulted in mild decreases in Ki67 staining patterns, but AZD7762 markedly decreased the proliferative indices in tumors, consistent with antitumor activity in this model. This effect was similarly apparent in the combination AZD7762 and radiation-treated tumors.

Discussion

The development of targeted therapies requires an early response biomarker, and ADC can be used for this purpose. DW-MRI has been shown to be a useful noninvasive biomarker for evaluating early effects of anticancer therapies [15,25,26] and applicable to a wide variety of tumor models [27–31]. The applicability of DW-MRI relies in the sensitivity of the method to treatment-induced alterations in microscopic tissue structure and physiology, which are reflected in significant changes to water movement within the tumor microenvironment [32,33]. Recent studies have also revealed the clinical translatability of

DW-MRI for early treatment response assessment in patients with primary brain tumors [26,34,35]. In the present study, DW-MRI provided the ability to dynamically follow the response of single or combination treatments by serially observing changes in tumor ADC values. Thus, integration of DW-MRI into a clinical GBM trial to follow treatment response would be anticipated to be valuable for assessing overall effects of AZD7762 in GBM patients and could provide an opportunity to optimize initial regimens.

Outcomes in GBM are poor largely related to treatment resistance to radiation and genotoxic chemotherapy such as temozolomide, in part due to heightened DNA damage response repair mechanisms in GBM cells [11,36]. Classic models are that most cancers are impaired in one or more DNA damage response pathways, allowing them to proliferate more rapidly than most normal cells. However, there is accumulating evidence that treatment-refractory tumors have evolved enhanced DNA repair capabilities to circumvent death. In one study, Bartkova et al.

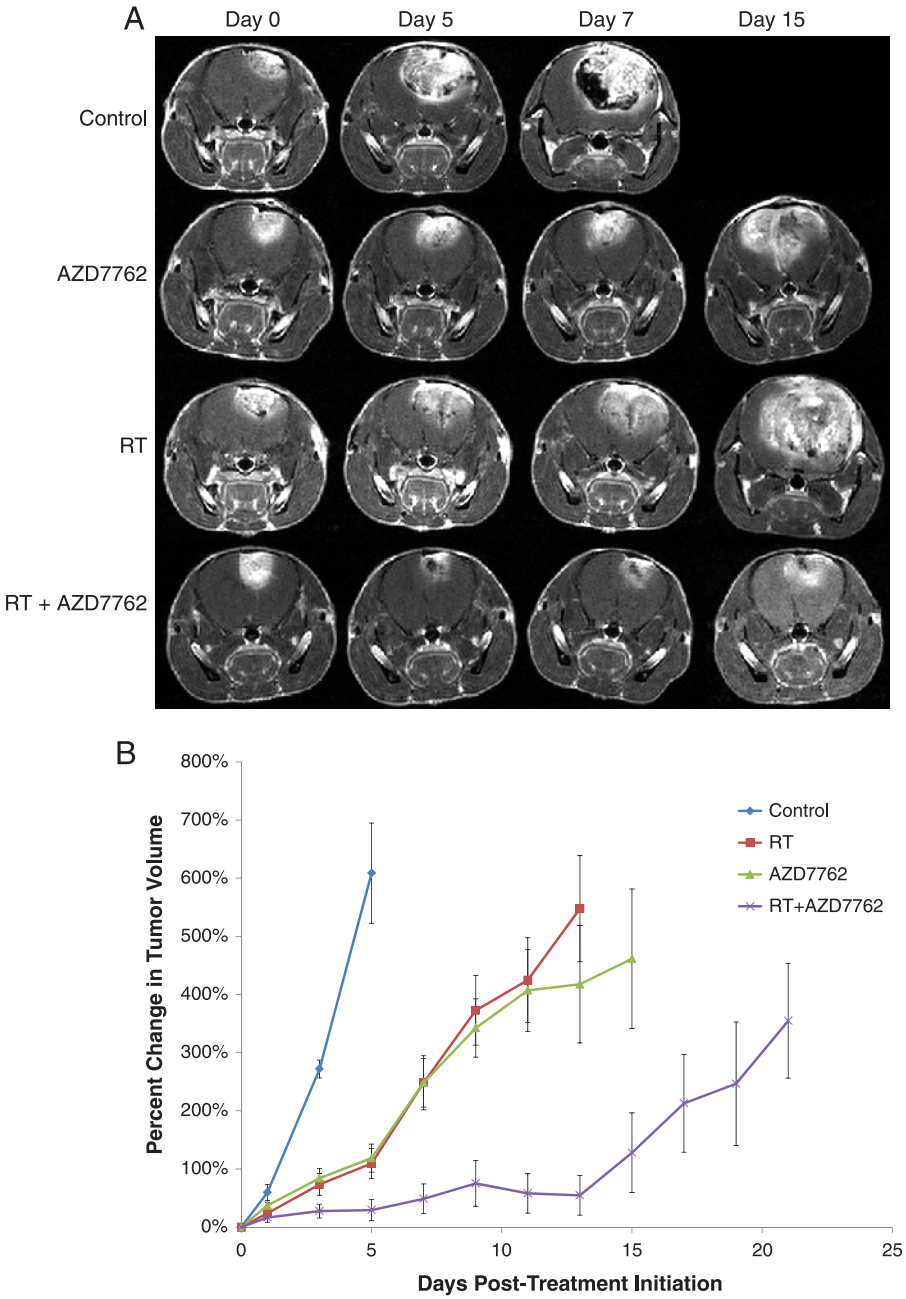

Figure 4. MR images and treatment response. (A) MRI data consist of anatomic contrast-enhancing coronal T1-weighted images for representative animals from each of the treatment groups from pretreatment (day 0) to days 5, 7, and 15. Day 15 is not shown for the control animal due to the rapid tumor growth for untreated animals. (B) MRI-determined intracerebral tumor volumes over time for each treatment group. Treatments occurred for 10 days total, 5 days/week. MRI was performed every other day during treatment and thereafter to determine tumor volume until end of study period for 1) control ($n = 7$), 2) 15 mg/kg AZD7762 ($n = 10$), 3) RT ($n = 10$), or 4) AZD7762 + RT ($n = 12$). Error bars represent SEM. All tumor volumes were significantly different ($P < .05$) from control tumor volumes beginning at day 3 posttreatment initiation. The combined therapy group was also significantly different ($P < .05$) from the other three groups beginning at day 3 posttreatment initiation.

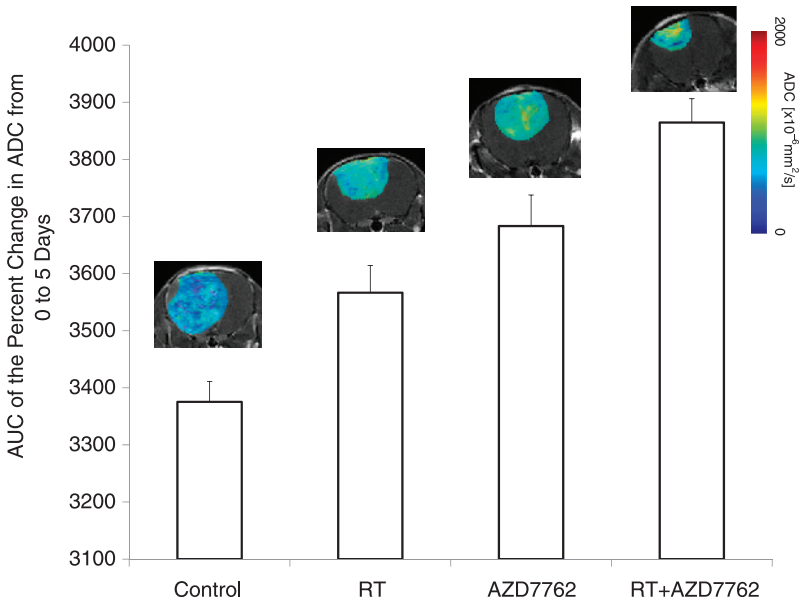

Figure 5. DW-MRI during the first 5 days of posttreatment initiation. The mean DW-MRI–derived ADC values for each of the treatment groups were obtained by AUC analysis of tumor ADC values from pretreatment to day 5 posttreatment initiation. Error bars represent SEM. RT and AZD7762 treatment groups were significantly different from the control group and the RT + AZD7762 group was significantly different from the ionizing radiation (IR; $P < .001$), AZD7767 ($P < .02$), and control ($P < .001$) groups at day 5. Color ADC overlay maps from representative tumors treated for 5 days are shown for each of the individual groups.

found increased levels of activated ATM, Chk2, and p53 in early tumorigenesis, suggesting heightened DNA repair mechanisms to counteract the genomic and mitotic stress encountered by tumors during rapid proliferation [37]. In GBM, this was nicely demonstrated in a report by Bao et al., which showed that glioma stem cells display an overexuberant DNA damage repair pathway and are resistant to radiation [11]. Furthermore, they also demonstrated that this effect was partly dependent on checkpoint kinases. Therefore, we hypothesized that targeting Chk1/2 kinases could serve to enhance the effects of radiation or genotoxic chemotherapy in glioma cells.

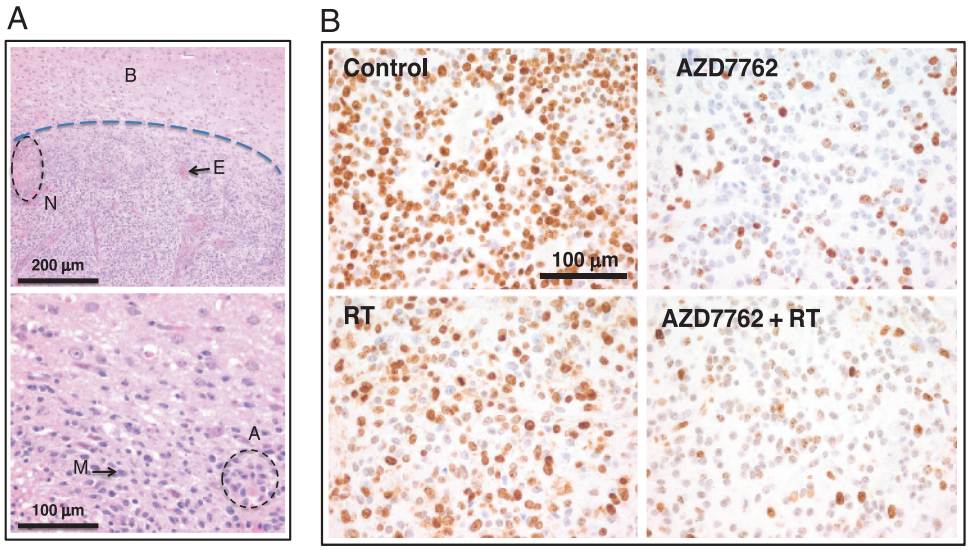

Figure 6. Histologic effects of AZD7762. (A) H&E-stained sections of control (vehicle-treated) tumors isolated at the end of the treatment schedule. The dashed line in the top panel represents that border between normal brain tissue (B) and the tumor. Tumors display typical hallmarks of human GBM, including areas of necrosis (N), endothelial proliferation (E), mitoses (M), and atypia (A). Top panel represents images taken at ×10 magnification, while the bottom panel is ×40. (B) Ki67 staining performed on tumor sections isolated from day 2 for the different treatment groups from Figure 4*B* ($n = 4$ per treatment group). Representative images are shown. Control (vehicle) tumors demonstrated high levels of Ki67-positive cells. RT induced modest decreases in Ki67 staining. However, treatment with AZD7762 resulted in marked decreases in the proportion of Ki67-positive cells. Sold bars are provided for magnification.

We now have a much better understanding of the genomic landscape of GBM [9,10,38]. It is well established that p53 mutations are common in primary and secondary GBM, occurring with a frequency of about 25% to 40% and 65% to 80%, respectively. Among its many functions, the tumor suppressor p53 is responsible for activating cell cycle arrest particularly at the G_1 checkpoint, to allow time for DNA repair in response to radiation or DNA-damaging chemotherapy. In p53-mutated tumors, cells rely more heavily on S and G_2 phase checkpoints to repair DNA damage after treatment. Thus, inactivation of the S and G_2 checkpoints represents an application of the synthetic lethality concept to enhance tumor cell kill.

Among many cell cycle regulators, checkpoint kinases 1 and 2 (Chk1 and Chk2) are critical for monitoring progression through S and G_2 phases [4–7]. These kinases act downstream of ATM and ATR kinases and possess important roles in cell cycle control, tissue development, and DNA damage repair. Upon activation, Chk1 becomes phosphorylated at Ser^{317} and Ser^{345} and undergoes autophosphorylation at Ser^{296}. These processes allow Chk1 to localize to the nucleus and exert its cell cycle regulatory functions. Activated Chk1 kinase phosphorylates cdc25A, targeting it for degradation, and phosphorylates cdc25C to invoke cell cycle arrest through blocking of cdc2. Chk2 is activated by ATM/ATR through phosphorylation of multiple sites by ATM/ATR kinases, regulates cdc25C phosphatase activity, and interacts with BRCA1 to restore survival after DNA damage [39,40].

AZD7762 is a potent and highly selective inhibitor of Chk1/2 kinases, which blocks cdc25A degradation, inactivates cdc25C, and allows cell cycle progression [20]. Thus, inhibiting S and G_2 phase checkpoints allows continued cell cycle progression and inability of cells to efficiently repair DNA damage, ultimately resulting in their death. We demonstrate here that treatment with AZD7762 results in reductions in GBM growth rates, clonal proliferation, and survival after radiation both *in vitro* and *in vivo*. We also demonstrate that these effects are maximal in p53-mutated cells.

Other groups have also shown the relative benefits of incorporating Chk1/2 inhibitors in combination with genotoxic compounds (e.g., gemcitabine and irinotecan) and/or radiation in other disease models, such as pancreatic, colon, prostate, and lung cancers [21,41]. Effective radiosensitization by checkpoint kinase inhibition also likely requires active movement through the cell cycle as has been demonstrated previously [41]. These findings also confirm the conclusions derived using pancreatic cancer–derived cell lines in that p53 mutant status resulted in the greatest degree of radiosensitization although p53 wild-type cells were also significantly sensitized compared to normal cells [41,42]. Furthermore, there is evidence that the presence of phosphorylated Chk1 (S345) may serve as a biomarker of AZD7762 response, with pChk1 (S345) levels increasing after treatment with AZD7762 [23]. Our findings corroborate this concept, with slight increased levels of pChk1 (S345) after AZD7762 treatment noted on immunoblots of U251 cells (Figure 1*B*).

As the standard treatment for GBM consists of surgery followed by a regimen of concurrent radiation and temozolomide, one must consider whether Chk1/2 inhibition can be incorporated into current standard of care. In GBMs, temozolomide appears to exert a G_2/M arrest in a p53-independent manner. In p53-proficient cells, prolonged treatment results in senescence, while p53-null cell treatment leads to mitotic catastrophe. Therefore, p53-deficient glioma cells appear more sensitive to the effects of temozolomide [43]. Since G_2/M arrest may protect cells from temozolomide-induced cytotoxicity, by allowing reversal of the cytotoxic effects of the drug for entry into mitosis and death by mitotic catastrophe, reversal of the G_2/M arrest may promote more sensitivity to temozolomide. In addition, it has been previously shown that temozolomide induces G_2/M arrest by activating Chk1 and Chk2, resulting in subsequent cdc25C and cdc2 phosphorylation [44,45]. Treatment with the Chk1 kinase inhibitor, UCN-01, potentiated temozolomide-mediated cytotoxicity by allowing cells to bypass G_2/M arrest and die from resulting mitotic catastrophe. This occurred in both p53-proficient and p53-deficient GBM cells [45]. Taken together, there is significant evidence that combining temozolomide and Chk1/2 is a rational approach for treating GBM.

In summary, we have demonstrated that radiation activates checkpoint kinases in GBM and that targeting Chk1/2 kinases results in substantial inhibition of GBM cell growth, while enhancing radiation efficacy in a panel of GBM cell lines as well as a transgenic GBM mouse model. The therapeutic effectiveness was enhanced in p53-mutated cells confirming our hypothesis that loss of p53 function enforces S and G_2 checkpoint dependency. Selectively targeting p53-deficient tumors with checkpoint kinase inhibition in combination with radiation thus would provide a greater therapeutic index that would serve to limit toxicity to normal tissues. Additionally, DW-MRI can play an important role in the preclinical development of novel therapeutic strategies directed against GBM. Our results provide rationale for exploring a regimen combining checkpoint kinase inhibition with radiation, optimally in p53-mutated GBM and for the integration of DW-MRI into the clinical trial protocol.

References

[1] Stupp R, Hegi ME, Mason WP, van den Bent MJ, Taphoorn MJ, Janzer RC, Ludwin SK, Allgeier A, Fisher B, Belanger K, et al. (2009). Effects of radiotherapy with concomitant and adjuvant temozolomide versus radiotherapy alone on survival in glioblastoma in a randomised phase III study: 5-year analysis of the EORTC-NCIC trial. *Lancet Oncol* **10**, 459–466.

[2] Keime-Guibert F, Chinot O, Taillandier L, Cartalat-Carel S, Frenay M, Kantor G, Guillamo JS, Jadaud E, Colin P, Bondiau PY, et al. (2007). Radiotherapy for glioblastoma in the elderly. *N Engl J Med* **356**, 1527–1535.

[3] Choudhury A, Cuddihy A, and Bristow RG (2006). Radiation and new molecular agents part I: targeting ATM-ATR checkpoints, DNA repair, and the proteasome. *Semin Radiat Oncol* **16**, 51–58.

[4] Sorensen CS, Syljuasen RG, Falck J, Schroeder T, Ronnstrand L, Khanna KK, Zhou BB, Bartek J, and Lukas J (2003). Chk1 regulates the S phase checkpoint by coupling the physiological turnover and ionizing radiation-induced accelerated proteolysis of Cdc25A. *Cancer Cell* **3**, 247–258.

[5] Xiao Z, Chen Z, Gunasekera AH, Sowin TJ, Rosenberg SH, Fesik S, and Zhang H (2003). Chk1 mediates S and G_2 arrests through Cdc25A degradation in response to DNA-damaging agents. *J Biol Chem* **278**, 21767–21773.

[6] Bartek J and Lukas J (2003). Chk1 and Chk2 kinases in checkpoint control and cancer. *Cancer Cell* **3**, 421–429.

[7] Ma CX, Janetka JW, and Piwnica-Worms H (2011). Death by releasing the breaks: CHK1 inhibitors as cancer therapeutics. *Trends Mol Med* **17**, 88–96.

[8] Smith J, Tho LM, Xu N, and Gillespie DA (2010). The ATM-Chk2 and ATR-Chk1 pathways in DNA damage signaling and cancer. *Adv Cancer Res* **108**, 73–112.

[9] Cancer Genome Atlas Research Network (2008). Comprehensive genomic characterization defines human glioblastoma genes and core pathways. *Nature* **455**, 1061–1068.

[10] Furnari FB, Fenton T, Bachoo RM, Mukasa A, Stommel JM, Stegh A, Hahn WC, Ligon KL, Louis DN, Brennan C, et al. (2007). Malignant astrocytic glioma: genetics, biology, and paths to treatment. *Genes Dev* **21**, 2683–2710.

[11] Bao S, Wu Q, McLendon RE, Hao Y, Shi Q, Hjelmeland AB, Dewhirst MW, Bigner DD, and Rich JN (2006). Glioma stem cells promote radioresistance by preferential activation of the DNA damage response. *Nature* **444**, 756–760.

[12] Ross BD, Zhao YJ, Neal ER, Stegman LD, Ercolani M, Ben-Yoseph O, and Chenevert TL (1998). Contributions of cell kill and posttreatment tumor growth

rates to the repopulation of intracerebral 9L tumors after chemotherapy: an MRI study. *Proc Natl Acad Sci USA* **95**, 7012–7017.

[13] Thoeny HC and Ross BD (2010). Predicting and monitoring cancer treatment response with diffusion-weighted MRI. *J Magn Reson Imaging* **32**, 2–16.

[14] Le Bihan D (1995). Molecular diffusion, tissue microdynamics and microstructure. *NMR Biomed* **8**, 375–386.

[15] Chenevert TL, McKeever PE, and Ross BD (1997). Monitoring early response of experimental brain tumors to therapy using diffusion magnetic resonance imaging. *Clin Cancer Res* **3**, 1457–1466.

[16] Buijs M, Kamel IR, Vossen JA, Georgiades CS, Hong K, and Geschwind JF (2007). Assessment of metastatic breast cancer response to chemoembolization with contrast agent enhanced and diffusion-weighted MR imaging. *J Vasc Interv Radiol* **18**, 957–963.

[17] Cui Y, Zhang XP, Sun YS, Tang L, and Shen L (2008). Apparent diffusion coefficient: potential imaging biomarker for prediction and early detection of response to chemotherapy in hepatic metastases. *Radiology* **248**, 894–900.

[18] Dudeck O, Zeile M, Pink D, Pech M, Tunn PU, Reichardt P, Ludwig WD, and Hamm B (2008). Diffusion-weighted magnetic resonance imaging allows monitoring of anticancer treatment effects in patients with soft-tissue sarcomas. *J Magn Reson Imaging* **27**, 1109–1113.

[19] Dzik-Jurasz A, Domenig C, George M, Wolber J, Padhani A, Brown G, and Doran S (2002). Diffusion MRI for prediction of response of rectal cancer to chemoradiation. *Lancet* **360**, 307–308.

[20] Zabludoff SD, Deng C, Grondine MR, Sheehy AM, Ashwell S, Caleb BL, Green S, Haye HR, Horn CL, Janetka JW, et al. (2008). AZD7762, a novel checkpoint kinase inhibitor, drives checkpoint abrogation and potentiates DNA-targeted therapies. *Mol Cancer Ther* **7**, 2955–2966.

[21] Morgan MA, Parsels LA, Zhao L, Parsels JD, Davis MA, Hassan MC, Arumugarajah S, Hylander-Gans L, Morosini D, Simeone DM, et al. (2010). Mechanism of radiosensitization by the Chk1/2 inhibitor AZD7762 involves abrogation of the G_2 checkpoint and inhibition of homologous recombinational DNA repair. *Cancer Res* **70**, 4972–4981.

[22] Galban S, Lemasson B, Williams TM, Li F, Heist KA, Johnson TD, Leopold JS, Chenevert TL, Lawrence TS, Rehemtulla A, et al. (2012). DW-MRI as a biomarker to compare therapeutic outcomes in radiotherapy regimens incorporating temozolomide or gemcitabine in glioblastoma. *PLoS One* **7**, e35857.

[23] Parsels LA, Qian Y, Tanska DM, Gross M, Zhao L, Hassan MC, Arumugarajah S, Parsels JD, Hylander-Gans L, Simeone DM, et al. (2011). Assessment of chk1 phosphorylation as a pharmacodynamic biomarker of chk1 inhibition. *Clin Cancer Res* **17**, 3706–3715.

[24] Lee KC, Hall DE, Hoff BA, Moffat BA, Sharma S, Chenevert TL, Meyer CR, Leopold WR, Johnson TD, Mazurchuk RV, et al. (2006). Dynamic imaging of emerging resistance during cancer therapy. *Cancer Res* **66**, 4687–4692.

[25] Chenevert TL, Meyer CR, Moffat BA, Rehemtulla A, Mukherji SK, Gebarski SS, Quint DJ, Robertson PL, Lawrence TS, Junck L, et al. (2002). Diffusion MRI: a new strategy for assessment of cancer therapeutic efficacy. *Mol Imaging* **1**, 336–343.

[26] Chenevert TL, Stegman LD, Taylor JM, Robertson PL, Greenberg HS, Rehemtulla A, and Ross BD (2000). Diffusion magnetic resonance imaging: an early surrogate marker of therapeutic efficacy in brain tumors. *J Natl Cancer Inst* **92**, 2029–2036.

[27] Hakumaki JM, Poptani H, Puumalainen AM, Loimas S, Paljarvi LA, Yla-Herttuala S, and Kauppinen RA (1998). Quantitative ^{1}H nuclear magnetic resonance diffusion spectroscopy of BT4C rat glioma during thymidine kinase-mediated gene therapy *in vivo*: identification of apoptotic response. *Cancer Res* **58**, 3791–3799.

[28] Hamstra DA, Lee KC, Tychewicz JM, Schepkin VD, Moffat BA, Chen M, Dornfeld KJ, Lawrence TS, Chenevert TL, Ross BD, et al. (2004). The use of ^{19}F spectroscopy and diffusion-weighted MRI to evaluate differences in gene-dependent enzyme prodrug therapies. *Mol Ther* **10**, 916–928.

[29] Poptani H, Puumalainen AM, Grohn OH, Loimas S, Kainulainen R, Yla-Herttuala S, and Kauppinen RA (1998). Monitoring thymidine kinase and ganciclovir-induced changes in rat malignant glioma *in vivo* by nuclear magnetic resonance imaging. *Cancer Gene Ther* **5**, 101–109.

[30] Stegman LD, Rehemtulla A, Hamstra DA, Rice DJ, Jonas SJ, Stout KL, Chenevert TL, and Ross BD (2000). Diffusion MRI detects early events in the response of a glioma model to the yeast cytosine deaminase gene therapy strategy. *Gene Ther* **7**, 1005–1010.

[31] Zhao M, Pipe JG, Bonnett J, and Evelhoch JL (1996). Early detection of treatment response by diffusion-weighted ^{1}H-NMR spectroscopy in a murine tumour *in vivo*. *Br J Cancer* **73**, 61–64.

[32] Evelhoch JL, Gillies RJ, Karczmar GS, Koutcher JA, Maxwell RJ, Nalcioglu O, Raghunand N, Ronen SM, Ross BD, and Swartz HM (2000). Applications of magnetic resonance in model systems: cancer therapeutics. *Neoplasia* **2**, 152–165.

[33] Rowley HA, Grant PE, and Roberts TP (1999). Diffusion MR imaging. Theory and applications. *Neuroimaging Clin N Am* **9**, 343–361.

[34] Hamstra DA, Chenevert TL, Moffat BA, Johnson TD, Meyer CR, Mukherji SK, Quint DJ, Gebarski SS, Fan X, Tsien CI, et al. (2005). Evaluation of the functional diffusion map as an early biomarker of time-to-progression and overall survival in high-grade glioma. *Proc Natl Acad Sci USA* **102**, 16759–16764.

[35] Moffat BA, Chenevert TL, Lawrence TS, Meyer CR, Johnson TD, Dong Q, Tsien C, Mukherji S, Quint DJ, Gebarski SS, et al. (2005). Functional diffusion map: a noninvasive MRI biomarker for early stratification of clinical brain tumor response. *Proc Natl Acad Sci USA* **102**, 5524–5529.

[36] Hegi ME, Diserens AC, Gorlia T, Hamou MF, de Tribolet N, Weller M, Kros JM, Hainfellner JA, Mason W, Mariani L, et al. (2005). MGMT gene silencing and benefit from temozolomide in glioblastoma. *N Engl J Med* **352**, 997–1003.

[37] Bartkova J, Horejsi Z, Koed K, Kramer A, Tort F, Zieger K, Guldberg P, Sehested M, Nesland JM, Lukas C, et al. (2005). DNA damage response as a candidate anti-cancer barrier in early human tumorigenesis. *Nature* **434**, 864–870.

[38] Verhaak RG, Hoadley KA, Purdom E, Wang V, Qi Y, Wilkerson MD, Miller CR, Ding L, Golub T, Mesirov JP, et al. (2010). Integrated genomic analysis identifies clinically relevant subtypes of glioblastoma characterized by abnormalities in PDGFRA, IDH1, EGFR, and NF1. *Cancer Cell* **17**, 98–110.

[39] Chehab NH, Malikzay A, Appel M, and Halazonetis TD (2000). Chk2/hCds1 functions as a DNA damage checkpoint in G_1 by stabilizing p53. *Genes Dev* **14**, 278–288.

[40] Lee JS, Collins KM, Brown AL, Lee CH, and Chung JH (2000). hCds1-mediated phosphorylation of BRCA1 regulates the DNA damage response. *Nature* **404**, 201–204.

[41] Mitchell JB, Choudhuri R, Fabre K, Sowers AL, Citrin D, Zabludoff SD, and Cook JA (2010). *In vitro* and *in vivo* radiation sensitization of human tumor cells by a novel checkpoint kinase inhibitor, AZD7762. *Clin Cancer Res* **16**, 2076–2084.

[42] Vance S, Liu E, Zhao L, Parsels JD, Parsels LA, Brown JL, Maybaum J, Lawrence TS, and Morgan MA (2011). Selective radiosensitization of p53 mutant pancreatic cancer cells by combined inhibition of Chk1 and PARP1. *Cell Cycle* **10**, 4321–4329.

[43] Hirose Y, Berger MS, and Pieper RO (2001). p53 effects both the duration of G_2/M arrest and the fate of temozolomide-treated human glioblastoma cells. *Cancer Res* **61**, 1957–1963.

[44] Chalmers AJ, Ruff EM, Martindale C, Lovegrove N, and Short SC (2009). Cytotoxic effects of temozolomide and radiation are additive- and schedule-dependent. *Int J Radiat Oncol Biol Phys* **75**, 1511–1519.

[45] Hirose Y, Berger MS, and Pieper RO (2001). Abrogation of the Chk1-mediated G_2 checkpoint pathway potentiates temozolomide-induced toxicity in a p53-independent manner in human glioblastoma cells. *Cancer Res* **61**, 5843–5849.